

# Kinetic, isotherm and thermodynamic aspects of Cu<sup>2+</sup> biosorption onto *Rosa damascena* leaf as a low-cost biosorbent: Optimization of process variables by Response Surface Methodology

Mustafa A. Fawzy (✉ [mafawzy@tu.edu.sa](mailto:mafawzy@tu.edu.sa))

Taif University

Hatim M. Al-Yasi

Taif University

Tarek M. Galal

Taif University

Reham Z. Hamza

Taif University

Esmat F. Ali

Taif University

Tharwat G. Abdelkader

Taif University

---

## Research Article

### Keywords:

**Posted Date:** December 6th, 2021

**DOI:** <https://doi.org/10.21203/rs.3.rs-1120602/v1>

**License:**   This work is licensed under a Creative Commons Attribution 4.0 International License.

[Read Full License](#)

---

<b>Kinetic, isotherm and thermodynamic aspects of Cu<sup>2+</sup> biosorption onto <i>Rosa</i></b>	1
<b><i>damascena</i> leaf as a low-cost biosorbent: Optimization of process variables by</b>	2
<b>Response Surface Methodology</b>	3
<b>Mustafa A. Fawzy*, Hatim M. Al-Yasi, Tarek M. Galal, Reham Z. Hamza, Esmat</b>	4
<b>F. Ali, Tharwat G. Abdelkader</b>	5
Department of Biology, College of Science, Taif University, P.O. Box 11099, Taif	6
21944, Saudi Arabia.	7
*Corresponding author, Email: <a href="mailto:mafawzy@tu.edu.sa">mafawzy@tu.edu.sa</a> , Phone (+9665594732248),	8
(+201002931424)	9
	10
	11
	12
	13
	14
	15
	16
	17
	18
	19
	20
	21
	22
	23
	24
	25

**Abstract** 26

In this study, the *Rosa damascena* leaf powder was evaluated as a biosorbent for 27  
copper removal from aqueous solutions. Optimized conditions of 4.0 g/L biosorbent 28  
dosage, pH of 5.5 and initial copper concentration of 55 mg/L obtained by Response 29  
Surface Methodology were employed for Cu<sup>2+</sup> biosorption by *R. damascena* leaves 30  
and up to 88.7 % Cu<sup>2+</sup> was removed. The biosorption data were well fitted to the 31  
pseudo-second order and Elovich kinetic models. The Langmuir and Dubinin- 32  
Radushkevich isotherm models were also best fit the experimental data showing 33  
monolayer isotherm with  $q_{max}$  value of 25.13 mg/g obtained at optimum conditions. 34  
Thermodynamic parameters showed the spontaneity, feasibility and exothermic nature 35  
of adsorption. Scanning electron microscopy, Energy-Dispersive X-Ray, and Fourier 36  
transform infrared spectroscopy were used to characterize the biosorbent before and 37  
after Cu<sup>2+</sup> biosorption, revealing outstanding structural characteristics and high 38  
surface functional groups availability. In addition, immobilized *R. damascena* leaves 39  
adsorbed 90.7 % of copper from aqueous solution, which is greater than free 40  
biosorbent (85.3 %). It can be concluded that *R. damascena* might be employed as a 41  
low-cost biosorbent for removing heavy metals from aqueous solutions. 42

**Keywords:** *Rosa damascena* leaves; Box–Behnken design; Copper; Isotherms; 43  
Kinetics; Thermodynamics. 44

**Introduction** 45

With the development of agricultural, industrial activities, and other human activity, 46  
various types of generated heavy metals have been released into water, and water 47  
resources have been severely contaminated<sup>1</sup>. Heavy metal pollution has been a hot 48  
topic for a long time because of its difficulty in removal and high toxicity<sup>2</sup>. Copper 49  
and its composites are the most frequent heavy metal contaminants in the 50

environment, according to the Environmental Protection Agency<sup>3</sup>. Wastewater from 51  
mining companies, tanneries, metal plating plants and refineries are the most 52  
prevalent sources of copper<sup>4</sup>. 53  
Copper is a trace metal that is needed as a catalyst by numerous enzymes in living 54  
organisms. High quantities of copper, on the other hand, may be highly poisonous and 55  
cause major health concerns. Extreme ingestion of copper causes liver accumulation, 56  
which can lead to anemia, gastrointestinal issues, and renal difficulties<sup>5</sup>. Several 57  
strategies for heavy metals removal from wastewaters have been developed in recent 58  
years. Some of these approaches include solvent extraction, membrane filtration, 59  
chemical reduction and precipitation, coagulation and ion exchange. The primary 60  
drawbacks of these procedures include the need for significant chemical amounts, 61  
residual metal solubility, costly capital investment, high operating costs, and the 62  
formation of a huge quantity of sludge<sup>6</sup>. Adsorption is a potential processing approach 63  
in terms of cost and efficiency for treatment of wastewater<sup>7</sup>. In recent research, a 64  
variety of typical agricultural waste products, microorganisms, algae, and natural 65  
polymers have been stated as excellent biosorbents for heavy metal removal<sup>8-10</sup>. 66  
Different parts of plants and their wastes are available and affordable when compared 67  
to chemically modified products. As a result, the majority of adsorption research has 68  
focused on untreated plant products and wastes<sup>11-12</sup>. 69  
Roses are cultivated as significant shrubs all over the world. These are decorative 70  
plants that are also utilized in medicine, fragrances, and scented products. Rose water, 71  
rose oil, and rose waste biomass are the three products of rose distillation<sup>13</sup>. Rose oil 72  
is made after distilling rose petals that is a blend of essential volatile oils. Rose oil is 73  
produced from two principal species of rose: Firstly, *Rosa damascena* which is 74  
commonly grown in China, India, Russia, Turkey, Spain, Italy, Bulgaria, and Saudi 75

Arabia. *Rosa centifolia*, which is more widely cultivated in France, Morocco, and 76  
Egypt, is the second species. Roses are widely grown in Saudi Arabia's governorates 77  
of Riyadh, Tabuk, Yanbu, and Taif. The Taif's rose is a widely distributed and 78  
cultivated plant in Saudi Arabia's cold and moderate regions. Because of the soil 79  
temperature and climate, the Taif's rose has a high-quality fragrance. Rose flowers 80  
biomass as a biosorbent after distillation has been examined in a number of studies<sup>13-</sup> 81  
<sup>16</sup>. 82

Yet, to the best of our knowledge, no reports of Rose leaves being used as waste 83  
biomass for biosorption of heavy metals have been available. 84

As a result, *Rosa damascena* leaf powder was employed as a biosorbent to examine its 85  
efficiency in removing copper ions from aqueous solutions. A Response Surface 86  
Methodology (RSM) was used in the present study to optimize the examined 87  
response, providing significant advantages such as time, effort, and resource savings. 88

Three independent factors were optimized, including biosorbent dosage, pH, and 89  
initial Cu<sup>2+</sup> concentration, with the goal of maximizing copper removal by *Rosa* 90  
*damascena* leaf powder. Furthermore, to assess the efficiency of immobilized *Rosa* 91  
*damascena* biomass as a Cu<sup>2+</sup> ion biosorbent. Kinetic, equilibrium, and 92  
thermodynamic investigations were carried out to study more about the biosorbent 93  
nature and the biosorption process. The biosorbent was characterized by SEM, EDX 94  
and FTIR techniques. 95

## **Results and Discussion**

 96

### **Box–Behnken Experimental Design**

 97

A Box–Behnken design was utilized for decreasing the number of tests and predicting 98  
the best conditions for copper removal by *R. damascena* leaf powder. Seventeen 99  
experiments were carried out using a BBD with varied combinations of three 100

parameters at three levels in order to maximize removal of  $\text{Cu}^{2+}$  ions from aqueous 101  
solution. Table 1 illustrates the actual and predicted removal percentages of  $\text{Cu}^{2+}$  for 102  
the 17 runs of the employed design matrix. The results show that the copper removal 103  
percentage varies greatly depending on the independent parameters. The copper 104  
removal percentage by *R. damascena* leaves varied between 44.25 % and 87.68 %. In 105  
run 4, with a biosorbent dosage of 5 g/L, pH of 6, and initial  $\text{Cu}^{2+}$  concentration of 60 106  
mg/L, the maximum copper removal was obtained with a value of 87.68 %. Based on 107  
the Box–Behnken design results, a second order polynomial equation was created to 108  
characterize the relationship between the independent parameters and the response, 109  
and the final model generated by backward elimination of insignificant parameters is 110  
as follows (Eq. 4): 111

$$\text{Cu}^{2+} \text{ removal percentage} = 57.2 + 10.54A + 5.13B - 4.28C + 5.71A^2 \quad (4) \quad 112$$

Where: *A*, *B* and *C*: the biosorbent dosage, pH and initial concentration of copper 113  
ions, respectively. 114

Table 2 summarizes the results of the analysis of variance (ANOVA) for the 115  
established model. The model was highly statistically significant, as evidenced by the 116  
high *F*-value (10.26) and low *p*-value (< 0.001). Furthermore, the *F*-value of lack of 117  
fit was 1.69, suggesting that lack of fit is not significant (as the *p* value is larger than 118  
0.05) in comparison to the real pure error, and so the model validity may be 119  
affirmed<sup>17</sup>. 120

The determination coefficient ( $R^2$ ) and adjusted  $R^2$  were used to assess the model's fit. 121  
The  $R^2$  value ranges between 0 and 1.0, with values around 1.0 indicates that the 122  
model is more accurate. However, in certain conditions, a larger  $R^2$  value indicates 123  
that the model has a large number of insignificant variables, which expects poor 124  
response. As a result, the adjusted  $R^2$  was developed, which adjusts the value of  $R^2$  125

based on the number of variables and sample size in the model. The high value of  $R^2$  (0.87; Table 2) in this investigation implies that the actual and expected values are well correlated, and the model can explain 87.0 % of the variability in the response. The adjusted  $R^2$  of 0.80 agrees rather well with the  $R^2$  value of 0.87, indicating that the model is valid. The actual and expected results were highly correlated, with the adjusted  $R^2$  value being high and close to the predicted  $R^2$  value (Table 2). Moreover, the value of variation coefficient as an estimate for standard error was less than 10%, indicating that the model was reproducible<sup>18</sup>. The signal-to-noise ratio is defined by adequate precision. In this investigation, a ratio of 9.8 (higher than 4) was found to be sufficient signal<sup>19</sup>. As a result, the model may be utilized to explore the design space. So, biosorption studies may be conducted using the model.

#### **Effect of interactive variables**

In order to understand the interaction impacts of the factors on the investigated response, 3-D response surface plots were made using the second-order equation (4) (Fig. 1). Each plot depicts the impact of two independent factors on the response within the examined ranges, while all other factors are kept constant.

In Fig. (1a), 3-D plots depict the reciprocal interaction between biosorbent dosage and pH on  $\text{Cu}^{2+}$  removal by *R. damascena* leaves biomass. The data revealed that raising the biosorbent dosage improved the  $\text{Cu}^{2+}$  biosorption by *R. damascena* leaves. ANOVA findings also demonstrated that biosorbent dosage was significant and had a positive linear influence on the efficiency of copper removal ( $p= 0.0003$ ; Table 3). As the biosorbent dosage is increased, the number of binding sites on the surface of *R. damascena* leaves rises, resulting in a higher percentage of copper removal<sup>20</sup>. On the other hand, the elimination of copper by the *R. damascena* leaves is pH-dependent as well. The pH exhibited a significant positive linear influence on removal of copper by

*R. damascena* leaves, according to the ANOVA data (Table 3). When the pH was raised from 2.0 to 6.0, biosorption of  $\text{Cu}^{2+}$  increased. Whereas, the copper biosorption onto *R. damascena* leaves was minimal at lower pH levels. However, in the pH 6.0 range, the maximum removal efficiency was recorded. These findings are clarified by the fact that the surface charge of the biomass is positive at lower pH levels, which makes cation biosorption difficult. Meanwhile,  $\text{H}^+$  ions compete with copper ions for active site space, leading to reduced biosorption process. The competitive impact of  $\text{H}^+$  ions and electrostatic repulsions between cations and surface sites reduce as pH rises. As a result, metal biosorption rises<sup>21</sup>. Fawzy<sup>22</sup> stated that, pH 5.0 was shown to be the most effective for copper removal by *Codium vermilara*.

Fig. 1b depicts the mutual impacts of biosorbent dosage and initial copper concentration on the effectiveness of copper removal by *R. damascena* leaves. When the biosorbent dosage was increased from 1 to 5 g/L, the copper removal efficiency increased. More binding sites on the surface of *R. damascena* leaves become available to the copper ions as the biosorbent dosage increases, resulting in enhanced removal efficiency. At 5 g/L of biosorbent dosage, the optimal removal effectiveness of 79 % could be achieved. Generally, higher biosorbent dosage and lower copper concentrations improved biosorption process<sup>23</sup>.

As a result, raising the concentration of copper ions had a significant negative impact on  $\text{Cu}^{2+}$  ions removal (Table 3). Because more copper ions in the solution connected with the binding sites at lower copper concentrations, biosorption of  $\text{Cu}^{2+}$  ions gradually increased; however, as concentrations of copper increased, biosorption reduced due to biosorbent site saturation and a large number of ions competing for the residual binding sites in the biosorbent.

The joint influence of pH and initial Cu<sup>2+</sup> concentrations on the metal ions removal 175  
was also investigated in the pH range of 2- 6 and initial copper concentrations of 30- 176  
90 mg/L as shown in Fig. 1c. The findings revealed that the removal of copper ions 177  
decreases as the pH reduces. The ANOVA analysis revealed that biosorbent dosage 178  
was the most statistically significant factor that influence the removal of copper ( $p=$  179  
0.0003), followed by pH ( $p=$  0.03) and initial copper concentration ( $p<$  0.05; Table 3). 180

### **Validation of the optimized variables**

 181

The goal of the optimization was to find the optimal values for independent 182  
parameters for Cu<sup>2+</sup> ions elimination by *R. damascena* leaf powder. In terms of copper 183  
removal efficiency, the aim was to maximize copper removal efficiency to achieve the 184  
maximum optimal rate of Cu<sup>2+</sup> removal. The average value for Cu<sup>2+</sup> removal 185  
efficiency was compared to the expected value in triplicate experiments conducted 186  
under optimized conditions. With biosorbent dosage of 4.0 g/L, pH of 5.5, and initial 187  
copper concentration of 55 mg/L, the highest expected Cu<sup>2+</sup> elimination by *R.* 188  
*damascena* biomass could be achieved. The experimentally observed value of copper 189  
removal efficiency (88.7 %) was found to be in accordance with the expected value 190  
(87.4 %) presented by the design expert software, implying that the optimized 191  
conditions were rational and trustworthy. 192

### **Kinetic models**

 193

The impact of contact time on the Cu<sup>2+</sup> ions biosorption was used to evaluate the 194  
kinetics process. Copper biosorption was examined under optimal conditions of 4.0 195  
g/L biosorbent dosage, pH 5.5, and initial Cu<sup>2+</sup> concentration of 55 mg/L by altering 196  
biosorption time from 0 to 150 minutes (Fig. 2a). In the first 30 minutes, the rate of 197  
Cu<sup>2+</sup> ion elimination was obviously fast. But, after reaching equilibrium, the 198  
biosorption efficiency increased to a steady level, and within 90 minutes, over 85.5 % 199

of the total metal had been eliminated. The rate of adsorption and desorption are now 200  
in dynamic equilibrium, and no biosorption progress was seen after this optimal 201  
equilibrium duration<sup>24</sup>. Because copper ions came in contact with unoccupied surface 202  
biosorption sites, biosorption of copper was initially quicker; however, as the 203  
equilibrium reached 90 minutes, the biosorption sites became saturated, and no further 204  
biosorption was allowed<sup>25</sup>. 205

Various kinetic models might be used to explain the mechanism and rate of metal ion 206  
sorption<sup>26</sup>. The biosorption kinetics of copper ions on *R. damascena* leaf biomass was 207  
studied using pseudo-first order, pseudo-second order, Elvoish, and Intra-particle 208  
diffusion models. 209

#### **Pseudo-first order kinetic model** 210

This model suggests adsorption of one adsorbate molecule onto one active site of the 211  
biosorbent. It is expressed as follows: 212

$$\text{Log} (q_e - q_t) = \text{Log} q_e - \frac{K_1 t}{2.303} \quad (5) \quad 213$$

Where  $q_e$  and  $q_t$  (mg/g): the quantity of copper ions absorbed by the biomass of *R.* 214  
*damascena* at equilibrium and at any time, respectively, and  $K_1$  ( $\text{min}^{-1}$ ): the pseudo- 215  
first order model's rate constant. 216

The constants of  $K_1$  and  $q_e$  were estimated from the slope and intercept of plotting log 217  
( $q_e - q_t$ ) vs. time, respectively (Fig. 2b). The high value of determination coefficient 218  
( $R^2 = 0.980$ ; Table 4), indicating that the experimental results accurately fit the 219  
pseudo-first order model for describing copper ion biosorption kinetics. However, the 220  
difference between the copper ions quantity biosorbed onto *R. damascena* surface 221  
estimated by experiments ( $q_{e \text{ exp.}}$ ; 17.1 mg/g) and the modeled value ( $q_{e \text{ calc.}}$ ; 13.4 222  
mg/g) were larger. It suggests to the fact that the biosorption process included both 223  
copper ions and biosorbent<sup>27</sup>. As a result, it is indicated that the pseudo-first order 224

model is unable to describe the experimental data of Cu<sup>2+</sup> biosorption onto the *R. damascena* biomass. The sorption kinetics of various metal ions onto various adsorbents has been described with similar findings<sup>15, 28-29</sup>.

The rate constant of pseudo-first order ( $K_1 = 0.029 \text{ min}^{-1}$ ; Table 4), is not a quantifiable value for clarifying the rapid equilibrium for biosorption of Cu<sup>2+</sup> ions onto *R. damascena* leaves surface reported within 30 minutes. As a result, this model was shown to be inadequate to accurately explain the order of copper biosorption by *R. damascena* biomass.

### **Pseudo-second order kinetic model**

The pseudo-second order kinetic model states that chemical adsorption, which includes the exchange or sharing of electrons between the adsorbate and the adsorbent, controls the process of adsorption. This model can be identified as follows

$$\frac{t}{q_t} = \frac{1}{K_2 q_e^2} + \frac{t}{q_e} \quad (6)$$

Where  $K_2$ : is the pseudo-second order model's rate constant (g/mg min), which may be used to calculate the initial rate of biosorption ( $h$ ; g/mg min).

$$h = K_2 q_e^2 \quad (7)$$

The kinetic constants of  $K_2$  and  $q_e$  were calculated from the intercept and slope of the  $t/q_t$  against  $t$  plot, respectively, (Fig. 2c).

The rate constant of pseudo-second order ( $K_2$ ) and initial rate of adsorption ( $h$ ) were 0.005 and 1.55 g/mg min, respectively (Table 4). At the beginning of the biosorption process, the  $h$  value was in good accordance with rapid biosorption of copper ions. Since the determination coefficient was determined to be 0.983, plots of pseudo-second order model showed strong linearity with the experimental data (Table 4). As well as, the experimental  $q_e$  (17.1 mg/g) is near to the calculated  $q_e$  (18.6 mg/g). Therefore, pseudo-second order was chosen as the best fit model, demonstrating

significant interactions between the adsorbate and the adsorbent, indicating the presence of copper chemisorption on the surface of *R. damascena* leaves. Several results support the pseudo-second order model for adsorption of copper ions by different biosorbents, including adsorption of  $\text{Cu}^{2+}$  onto activated rubber wood sawdust<sup>30</sup>, *Tectona grandis* leaf<sup>31</sup>, sour orange residue<sup>32</sup>, banana trunk fiber<sup>33</sup>, sulfur-modified bamboo powder<sup>34</sup>, *Platanus orientalis* leaf powder<sup>35</sup>.

### **Elovich model**

The Elovich model was utilized to explain the kinetics of chemical adsorption of a gas by solid adsorbents, but it was proven to be effective in various types of adsorption.

The Elovich model can be represented by the following equation:

$$q_t = \frac{1}{\beta} \ln(\alpha\beta) + \frac{1}{\beta} \ln(t) \quad (8)$$

Where,  $\alpha$  (mg/g min): the initial rate of sorption process, and  $\beta$  (g/mg): the constant of desorption.

To study the mechanism of  $\text{Cu}^{2+}$  biosorption, the experimental data were fitted to the Elovich kinetic model (Fig. 2d). By plotting  $q_t$  versus  $\ln t$ , the Elovich constants ( $\alpha$  and  $\beta$ ) were determined from intercept and slope, respectively. The extent of chemisorption is proportional to the value of  $\alpha$ . The high value of Elovich constant ( $\alpha = 1.3$  g/mg min; Table 4), implying chemisorption is the rate-limiting stage and approving the pseudo-second order type of biosorption.

The lower the value of Elovich constant  $\beta$ , the lower chemisorption activation energy, implying quick adsorption<sup>36</sup>. In the current investigation, the  $\beta$  value is fairly low (0.303 g/mg), suggesting a reduced activation energy of chemical adsorption. In addition, the high value of determination coefficient ( $R^2 = 0.971$ ), showing that the experimental data fits well the Elovich kinetic model.

### **Intra-particle diffusion model**

The intra-particle diffusion kinetic model is related with the adsorbate diffusion to the inner pores as the rate-controlling step which is represented by eq. 9:

$$q_t = K_i t^{1/2} + C_i \quad (9)$$

Where  $K_i$  denotes the intra-particle diffusion rate constant ( $\text{mg/g min}^{0.5}$ ) and  $C_i$  denotes the intercept.

The biosorption of  $\text{Cu}^{2+}$  ions on *R. damascena* leaf surface was studied using an intra-particle diffusion kinetic model, which had a low  $R^2$  value (0.80; Table 4). The linear plot indicated in Fig. 2e does not pass through the origin, proposing that the intra-particle model is not the rate-limiting stage during the process of biosorption. Fig. 2e also exhibited the multilinearity of the plot, which has two steps. All of the points of experimental data found on two straight lines, with the first line indicating copper ions biosorption on the most available empty sites or the external surface (external diffusion) on the *R. damascena* leaf surface, and the second steep line indicating copper ions biosorption on internal pores (intra-particle diffusion)<sup>37</sup>.

### **Equilibrium Isotherms**

At a certain experimental conditions, the adsorption isotherm represents the equilibrium correlation between the amounts of ions adsorbed by the biosorbent and the metal ions concentration in solution<sup>38</sup>.

Biosorption equilibrium isotherms were performed under optimized conditions obtained by BBD. Langmuir, Freundlich, Temkin and Dubinin-Radushkevich isotherm models were developed to describe and estimate the experimental data of copper biosorption.

### **Langmuir model**

This model implies that metal ions are adsorbed by monolayer adsorption on a homogeneous surface with no interaction between the adsorbed metal ions. The Langmuir model is represented in linear form as follows:

$$\frac{C_{eq}}{q_e} = \frac{1}{q_{max}b} + \frac{C_{eq}}{q_{max}} \quad (10)$$

Where  $q_{max}$ : the maximal sorption quantity (mg/g) required to produce full monolayer coverage on *R. damascena's* surface at a high equilibrium ion concentration ( $C_{eq}$ ; mg/L), and  $b$ : the constant of Langmuir model, which is associated with binding site affinity<sup>39</sup>.

The high value of  $R^2$  (0.979; Table 5) indicated that Langmuir isotherm offers a suitable model of the biosorption process, which is based on homogeneous biosorption of copper ions by *R. damascena* leaf surface.

When  $C_{eq}/q_e$  was plotted versus  $C_{eq}$ , a straight line was formed, and the slope and intercept were used to determine the  $q_{max}$  and  $b$  values, respectively (Fig. 3a). The greater value of Langmuir constant ( $b= 0.095$  L/mg), suggesting a stronger interaction with the functional groups of *R. damascena* leaf surface. Furthermore, *R. damascena* biomass had a maximum biosorption capacity ( $q_{max}$ ) of 25.13 mg/g. *Rosa damascena* leaves are a very good biosorbent when compared to the capacity of other biosorbents occurred in the literature for copper removal. For example, dried marine green macroalga *Caulerpa lentillifera* has 5.57 mg/g<sup>40</sup>, lentil shell has 8.98 mg/g<sup>41</sup>, 14.4 mg/g for *Codium vermilara*<sup>22</sup> and 23.14 mg/g for dried bael flowers<sup>29</sup>.

A dimensionless separation factor ( $R_L$ ) may be used to determine the shape and favorability of the biosorption process, which can be computed using Eq. (11):

$$R_L = 1/(1 + bC_0) \quad (11)$$

Where  $C_0$ : the metal ion concentration (mg/L). The type of Langmuir isotherm was determined by the  $R_L$  value, which was either unfavorable ( $R_L > 1$ ), linear ( $R_L = 1$ ),

irreversible ( $R_L = 0$ ) or favorable ( $0 < R_L < 1$ )<sup>35</sup>. The value of  $R_L$  between 0 and 1 323  
indicate that the adsorption is favorable. In the current study, the  $R_L$  value was 324  
determined to be 0.062–0.201, showing that copper biosorption by the leaves of *R.* 325  
*damascena* is favorable (Table 5). 326

### **Freundlich isotherm model** 327

The adsorption of ions on an energetically heterogeneous surface is described by the 328  
Freundlich isotherm model. The following equation represents the linearized 329  
Freundlich model (12): 330

$$\ln q_e = \ln K_f + \frac{1}{n} \ln C_{eq} \quad (12) \quad 331$$

Where  $K_f$ : the Freundlich isotherm constant which reflects the sorption capacity, and 332  
 $n$ : the Freundlich constant correlated to the adsorption intensity. 333

The intercept and slope of the plotting of  $\ln q_e$  against  $\ln C_{eq}$  are used to calculate the 334  
 $K_f$  and  $1/n$  values, respectively (Fig. 3b). The greater the  $K_f$  value, the more biosorbent 335  
may be loaded. In addition, the adsorption is favorable when the  $1/n$  value is between 336  
0.1 and 1.0<sup>42</sup>. In this study, the value of  $1/n$  was lower than 1.0 (0.313; Table 5), 337  
indicating that biosorption of copper ions by *R. damascena* leaves is favorable. The 338  
low value of determination coefficient ( $R^2 = 0.735$ ) suggested that Freundlich model is 339  
not appropriate for describing the experimental data of biosorption process (Table 5). 340

### **Temkin model** 341

The adsorption in the Temkin model is supposed to be represented by a uniform 342  
distribution of binding energies up to the maximal binding energy, as shown in the 343  
following equation<sup>43</sup>. 344

$$q_e = B \ln A + B \ln C_{eq} \quad (13) \quad 345$$

$$B = \frac{RT}{b} \quad (14) \quad 346$$

Where  $A$  (L/mg): represents the equilibrium binding constant,  $b$  (J/mol): the constant of Temkin isotherm model, and  $B$  (J/mol): the heat of sorption constant.

The Temkin model constants ( $A$  and  $b$ ) were determined using the intercept and slope of the  $q_e$  versus  $\ln C_{eq}$  plotting (Fig. 3c). The high  $b$  value (551.4 J/mol; Table 5) indicates that the adsorbate and biosorbent surface interact strongly<sup>44</sup>. The Temkin model fails to explain the results reported for copper biosorption by *R. damascena* leaves, with copper exhibiting low value of  $R^2$  (0.807; Table 5). This demonstrates that biosorption of  $\text{Cu}^{2+}$  is exothermic in nature, with the adsorption heat of the molecules increasing linearly as the biosorbent surface is covered<sup>45</sup>.

#### **Dubinin–Radushkevich model (D–R)**

The D–R model describes the chemical or physical nature of biosorption process, as well as the mean sorption energy of the process. D–R model is calculated from the following Equations:

$$\ln q_e = \ln q_0 - \beta \varepsilon^2 \quad (15)$$

$$\varepsilon = RT \ln\left(1 + \frac{1}{C_{eq}}\right) \quad (16)$$

$$E = \sqrt{1/2}\beta \quad (17)$$

Where  $q_0$ : is the theoretical maximum capacity (mg/g),  $\beta$ : is the constant of D–R model associated with mean free energy ( $\text{mol}^2/\text{J}^2$ ),  $\varepsilon$ : Polanyi potential,  $T$  (K): the absolute temperature,  $R$  (8.314 J/mol K): the gas constant, and  $E$  (kJ/mol): the mean adsorption energy.

Table 5 shows the values of the D–R model parameters. The mean adsorption energy of the system ( $E$ ) was determined using the parameter  $\beta$  (eq. 17). In addition, the chemical and physical characteristics of the adsorption process may be assessed by the amount of mean adsorption energy.

Physical sorption is defined as a value of  $E$  less than 8 kJ/mol, whereas chemical sorption is defined as a value of 8 to 16 kJ/mol<sup>25</sup>. The value of  $E$  (9.13 kJ/mol) indicates that *R. damascena* removed copper ions mostly by chemisorption. This is also consistent with predictions from pseudo-second order and Elovich kinetic models.

From the previous data, it is concluded that, the Langmuir and D–R isotherm models may best describe the experimental data of copper ions biosorption onto *R. damascena* leaf surface, according to a comparison of  $R^2$  values (0.926; Fig. 3d; Table 5).

### Thermodynamic studies

Gibbs free energy ( $\Delta G$ ), enthalpy ( $\Delta H$ ) and entropy ( $\Delta S$ ) are all thermodynamic parameters that describe the spontaneity of a biphasic adsorption process<sup>46</sup>.

The following equations demonstrate the relationship between the thermodynamic parameters and absolute temperature ( $T$ )<sup>47</sup>.

$$\Delta G = \Delta H - T \Delta S \quad (18)$$

$$\Delta G = -RT \ln K_C \quad (19)$$

$$\ln K_C = \frac{\Delta S}{R} - \frac{\Delta H}{RT} \quad (20)$$

Where  $K_C$ : the equilibrium thermodynamic constant.

At the experimental temperatures, the values of  $\Delta G$  were negative (Table 6), indicating that the biosorption process was feasible and spontaneous<sup>47</sup>. Furthermore, the negative value of  $\Delta G$  indicated that the concentration of copper ions on the *R. damascena* leaf was significantly higher than that in the aqueous solution<sup>48</sup>. Also, its values revealed that as the temperature rose, so did the spontaneity.

The changes of enthalpy and entropy were evaluated from the slope and intercept of the  $\ln K$  versus  $1/T$  plot, respectively (Fig. 4).

The negative  $\Delta H$  value of 21.7 K/J mol for copper biosorption by *R. damascena* leaves indicates that biosorption process was exothermic. In addition, the positive  $\Delta S$  value indicated that biosorption of copper ions onto *R. damascena* leaf surface occurred as a result of randomization at the adsorbate-biosorbent interface<sup>49</sup>.

### **Characterization of *R. damascena* leaf surface**

#### **Scanning electron microscopy (SEM)**

The morphology of the *R. damascena* leaf surface before and after  $\text{Cu}^{2+}$  biosorption was examined by SEM (Fig. 5). SEM micrographs demonstrated that the surface morphology of the *R. damascena* leaf before and after  $\text{Cu}^{2+}$  biosorption was different. The SEM micrographs of the *R. damascena* leaf surface before copper biosorption revealed a rough surface with substantial porosity (Fig. 5a). This rough flaky surface allows copper ions to adhere more easily, improving the process of biosorption. The biosorbent's porosity also helps it interact with the adsorbate more quickly<sup>50</sup>. On the other hand, the SEM images after biosorption of copper revealed a flatter biosorbent surface, appearance of discrete lumps and vanishing of big spaces (Fig. 5b). These morphological alterations verified the interaction of copper ions with functional groups on the *R. damascena* leaf surface<sup>22</sup>.

#### **Energy dispersive X-ray spectroscopy (EDX)**

The EDX analysis was used to determine the adsorbent surface's composition as well as to confirm the presence of copper ions on the *R. damascena* leaf surface. Figure 6 displays the EDX spectra of *R. damascena* biomass. The EDX spectra showed that the *R. damascena* leaves consist mostly of C and O, with traces of additional elements including Na, Mg, Cl, K, Si and Ca that were exchanged or disappeared during the process of biosorption (Fig. 6a, b). This shows that biosorption of  $\text{Cu}^{2+}$  ions was caused by ion exchange. After biosorption, the EDX spectra of *R. damascena* biomass

exhibit an additional  $\text{Cu}^{2+}$  peak (1.09 %) on the *R. damascena* leaf surface, 421  
demonstrating that the biomass of *R. damascena* is participated in biosorption of  $\text{Cu}^{2+}$  422  
ions from solution (Fig. 6b). In this regard, El-Naggar et al.<sup>51</sup> observed that the 423  
distinctive copper peak appeared following contact with copper. 424

#### **Analysis of Fourier transform infrared spectra (FT-IR) 425**

The functional groups found on the surface of biosorbent biomass play a significant 426  
role in the process of adsorption. Heavy metal biosorption has been related to various 427  
functional groups such as sulfonate, sulfhydryl, amine, carboxyl, hydroxyl, carbonyl, 428  
and others<sup>52</sup>. Figure 7a, b displays the FT-IR spectra of *R. damascena* leaves before 429  
and after copper biosorption. 430

The presence of wide absorption peak at around  $3421\text{--}3425\text{ cm}^{-1}$  is allocated to O–H 431  
stretching of hydroxyl radicals of polysaccharides or water<sup>53</sup>, and to N–H stretching of 432  
proteins (amide A)<sup>54</sup>. The functional groups such as O–H and N–H are commonly 433  
present in natural cellulose and proteins found in plant cell walls<sup>55</sup>. The O–H 434  
stretching vibration of the carboxylic acid might be represented by the bands at  $2921$  435  
 $\text{cm}^{-1}$  and  $2922\text{ cm}^{-1}$ <sup>55</sup>. This refers to the existence of an acidic group in the biosorbent 436  
cell wall, such as  $\text{-COOH}$ , which serves as a hyper chemical group for the adsorption 437  
of various multivalent metal ions<sup>56</sup>. Absorption bands at  $2852\text{ cm}^{-1}$  and  $2853\text{ cm}^{-1}$  are 438  
allocated to stretching of C–H, more specifically to C–H stretching vibrations of 439  
lipids<sup>57</sup>. The C=O stretching of amide I, which is related with proteins, is shown by 440  
the absorption peak at around  $1654\text{ cm}^{-1}$ <sup>58</sup>. After copper biosorption onto the *R.* 441  
*damascena* leaf surface, the appearance of new absorption bands at  $1546\text{ cm}^{-1}$  and 442  
 $1460\text{ cm}^{-1}$  might be attributed to C=O stretching vibration in different carboxylic and 443  
amide (I, II) groups, respectively<sup>59</sup>. The protein band spectrum identified at  $1240\text{ cm}^{-1}$  444  
on the leaf surface was caused by the P=O asymmetric stretching vibration<sup>60</sup>. The 445

absorption peak at about  $1160\text{ cm}^{-1}$  detected only on the *R. damascena* leaf surface 446  
following copper biosorption is related to C–O–C stretching of polysaccharides from 447  
carbohydrates<sup>53</sup>. Furthermore, after copper biosorption, the peak at  $878\text{ cm}^{-1}$  shifts to 448  
 $893\text{ cm}^{-1}$ , indicating binding of copper ions to the amine group on the leaf surface. 449  
The band found only at  $670$  and  $593\text{ cm}^{-1}$  onto the *R. damascena* leaf surface after 450  
copper biosorption may be associated with the compounds of organic halide<sup>52</sup>. From 451  
the Fig. 7, it can be observed that the *R. damascena* leaf biomass included several 452  
functional chemical groups such as carbonyl, acids, phosphate, amides, hydroxyl, 453  
halides, carboxyl, and amine groups. They might compensate the biosorption of 454  
copper ions onto *R. damascena* leaf surface from the aqueous solution. 455

#### **Copper removal by immobilized *R. damascena* biomass** 456

The results in Fig. 8 showed that the Ca-alginate immobilized *R. damascena* leaves 457  
removed 90.7 % of copper ions after 120 minutes under optimized conditions 458  
obtained by BBD such as biosorbent dosage (4 g/L), pH (5.5) and initial copper 459  
concentration (55 mg/L), which was higher than the removal shown using non- 460  
immobilized biosorbent (85.3 %). Various studies stated that immobilized biosorbent 461  
has the ability to use a straightforward approach for recovering and removing heavy 462  
metals from wastewater, in comparison to free biosorbent<sup>61-62</sup>. In this regard, Ansari et 463  
al.<sup>15</sup> reported that immobilized rose waste is more effective than free biomass at 464  
absorbing  $\text{Pb}^{2+}$  from aqueous solutions. Ca-alginate immobilized *Fucus vesiculosus* is 465  
also an effective biosorbent for copper, lead, and cadmium according to Mata et al.<sup>63</sup>, 466  
with sometimes greater biosorption efficacy than free alga or even alginate alone. 467  
According to Davis et al.<sup>64</sup>, the metal ions affinity for alginate is proportional to the 468  
quantity of guluronic acid and other uronic acids present. These acids are responsible 469  
for biosorption of heavy metals since they include the majority of the carboxyl groups 470

in alginate. Furthermore, the “egg-box” structure of the gels, as well as crosslinking 471  
between carboxyl groups and metal ions have been linked to alginate's metal 472  
selectivity. This selectivity is determined by the stereochemical environment created 473  
by the structure of the gel. Therefore, *R. damascena* immobilized in Ca-alginate has a 474  
great potential for adsorption of heavy metals from wastewater. 475

## **Conclusions** 476

The Box–Behnken experimental design has been shown to be an effective method for 477  
maximizing the removal of copper ions from solutions using the *R. damascena* leaf by 478  
decreasing the number of experimental tests, expecting the highest efficiency 479  
conditions, and keeping a good accuracy of the predicted response. The maximum 480  
removal percentage of  $\text{Cu}^{2+}$  ions (88.7%) was reached under optimal conditions of 481  
biosorbent dose of 4.0 g/L, pH of 5.5, and initial copper content of 55 mg/L. The 482  
pseudo-second order and Elovich kinetic models were best fit to the experimental 483  
data. Furthermore, the equilibrium isotherm studies demonstrated that the D–R and 484  
Langmuir isotherm models could better describe  $\text{Cu}^{2+}$  biosorption than the Freundlich 485  
and Temkin models with a highest monolayer biosorption capacity of 25.13 mg/g, 486  
suggesting the chemical interaction between the metal ions and biosorbent. The 487  
thermodynamics parameters such as Gibbs free energy and enthalpy, as well as 488  
entropy, showed that the biosorption process is spontaneous and exothermic. As a 489  
result of the biosorption process, SEM and EDX tests indicated noticeable alterations 490  
in the properties of the *R. damascena* leaf surface. In addition, FT-IR investigations 491  
revealed the existence of functional groups in the *R. damascena* leaves biomass such 492  
as carbonyl, acids, phosphate, amide, hydroxyl, halide, carboxyl, and amine groups, 493  
all of which are likely to be involved in biosorption of copper ions. Immobilization 494  
was shown to be a promising method for producing efficient adsorbents, which might 495

be used to sequester metal ions from wastewater. Therefore, <i>R. damascena</i> leaves can	496
be used as a low-cost biosorbent to remove copper ions from aqueous solutions.	497
<b>Materials and methods</b>	498
<b>Preparation of biosorbent</b>	499
<i>Rosa damascena</i> Miller var. <i>trigintipetala</i> Dieck was collected from Taif rose farms at	500
Al-Shafa highland, Taif region, Saudi Arabia. Voucher specimens were deposited and	501
identified by staff members of the herbarium of Taif University, Taif, Saudi Arabia.	502
The leaves of the rose plant were removed off the plant, washed under running water	503
to eliminate any impurities or pollutants, and then dried at room temperature for two	504
weeks. For further investigation, the leaves were crushed into fine powder and kept in	505
an airtight container.	506
<b>Preparation of copper solutions</b>	507
About 3.93 g copper sulphate ( $\text{CuSO}_4 \cdot 5\text{H}_2\text{O}$ ) was dissolved in 1000 mL distilled	508
water to prepare the $\text{Cu}^{2+}$ stock solution. All of the chemicals used in this	509
investigation were analytical grade and obtained from Sigma-Aldrich, including	510
$\text{CuSO}_4 \cdot 5\text{H}_2\text{O}$ , HCl, NaOH, Na-alginate and $\text{CaCl}_2$ .	511
<b>Optimization of <math>\text{Cu}^{2+}</math> removal by Box–Behnken statistical design (BBD)</b>	512
Response Surface Methodology is a multivariable optimization approach that fits	513
experimental results to a second-order equation to determine the optimal response of a	514
process that is a function of numerous independent factors. Designing an experimental	515
matrix, developing a mathematical model, and optimizing the response are the three	516
key processes of RSM <sup>65</sup> . Experiments were developed to determine the optimal	517
copper biosorption onto <i>R. damascena</i> leaves using Box–Behnken Design of RSM	518
(Stat-Ease Inc., Minneapolis, USA). The design includes 17 runs with three	519
independent factors such as biosorbent dosage (1, 3, 5 g/L), pH (2, 4, 6) and initial	520

copper concentration (30, 60, 90 mg/L), at three coded levels (-1, 0, +1) (Table 1). 521

The following equation is a second-order polynomial equation concerning the 522

independent factors and the dependent response. 523

$$Y = \beta_0 + \sum \beta_i X_i + \sum \beta_{ii} X_i^2 + \sum \beta_{ij} X_i X_j + \varepsilon \quad (1) \quad 524$$

Where  $Y$ : is the expected response,  $\beta_0$ : is the intercept term,  $\beta_i$ ,  $\beta_{ii}$  and  $\beta_{ij}$ : are the 525

linear, quadratic, and interaction impacts, respectively,  $X_i$  and  $X_j$ : are the independent 526

variables, and  $\varepsilon$ : is the error. 527

### **Statistical analysis of the data** 528

It has been stated that three-dimensional response surface plots may be used to 529

analyze the principal and interaction impacts of two parameters while keeping all 530

other variables constant. The regression model was used to produce the 3D response 531

surface plots for the copper removal percentage, by keeping one factor at the center 532

level. The experimental design and statistical analysis were done in Design Expert 533

version 7. Multiple regression analysis and ANOVA were used to assess the 534

experimental data, and the significance was determined at probability levels using the 535

$F$  test ( $p \leq 0.05$ ). 536

### **Biosorption experiments** 537

The tests were carried out in 250 mL conical flasks with 100 mL of copper solution, 538

which were agitated at 170 rpm in a shaker. All of the tests were achieved at a 539

temperature of 25 °C and a contact period of 90 minutes. Deionized water was used to 540

prepare the solutions, and the pH was adjusted using 0.1 M HCl or 0.1 M NaOH. 541

Each experiment was repeated three times, with the average results provided. The 542

biosorbent was removed from the solutions at the end of the biosorption procedure by 543

centrifugation for 5 minutes at 4000 rpm. 544

The concentration of copper in the filtrate was determined by Inductively Coupled Plasma-Optical Emission Spectrometer (ICP-OES) model Perkin Elmer Optima 2000 DV. The following equation is used to calculate the biosorption of copper ions onto *R. damascena* leaf biomass ( $q_e$ ; mg/g).

$$q_e = \frac{V(C_i - C_{eq})}{W} \quad (2)$$

Where  $C_i$  and  $C_{eq}$  (mg/L): the copper ion concentrations before and after the equilibrium contact time,  $V$  (mL): the volume of copper solution, and  $W$  (g): the weight of *R. damascena* leaf powder.

The removal percentage of  $\text{Cu}^{2+}$  ions by *R. damascena* leaves was calculated by the following Eq. (3):

$$\text{Removal (\%)} = \frac{(C_i - C_{eq})}{C_i} \times 100 \quad (3)$$

The optimized conditions obtained from BBD were used to determine the kinetic biosorption models at various time periods (0- 150 min), as well as to estimate isothermal models at varied initial  $\text{Cu}^{2+}$  concentrations (30, 60, 90, 120 and 150 mg/L) and contact time of 90 minutes at 25 °C. Thermodynamic investigations of  $\text{Cu}^{2+}$  ion biosorption were also examined, with the biosorption process being tested under optimal conditions at different temperatures (25, 35, and 45 °C).

### **Characterization of *R. damascena* leaves**

A scanning electron microscope (SEM– JEOL JSM-6510 L.V operated at 30 KV) with energy–dispersive X–ray spectroscopy (EDX, JEOL JEM-2100 (HRTEM) operated at a voltage of 200 KV) was used to examine the surface morphology of the *R. damascena* leaves. The functional groups on the *R. damascena* leaf surface were determined using Fourier transform infrared radiation (FTIR, Thermo Fisher Scientific model FT-IR is 10, USA) before and after biosorption process.

### **Biosorbent immobilization**

*Rosa damascena* leaf was immobilized for 30 minutes at 60 °C with continual stirring 570  
by dissolving 4 g of Na-alginate in 100 mL distilled water<sup>66</sup>. In a Na-alginate solution, 571  
4 g/L of *R. damascena* leaf powder was added. This mixture was then put into a 2 % 572  
CaCl<sub>2</sub> solution using a 3 mL syringe for formation of beads. For full gelation, the 573  
spherical beads (3 mm) were maintained for 2 hours in a 2 % calcium chloride 574  
solution. The beads were then rinsed in distilled water to eliminate any excess CaCl<sub>2</sub> 575  
and kept in the refrigerator until they were needed again. The biosorption experiment 576  
was performed as previously described utilizing immobilized *R. damascena* leaves 577  
and non-immobilized biosorbent as a control under optimum conditions obtained by 578  
BBD at a temperature of 25 °C and various time intervals (0- 150 min). 579  
All methods were performed in accordance with relevant guidelines and regulations. 580

## References 581

1. Yu, S. *et al.* Macroscopic, spectroscopic, and theoretical investigation for the 582  
interaction of phenol and naphthol on reduced graphene oxide. *Environ. Sci.* 583  
*Technol.* **51**(6), 3278-3286 (2017). 584
2. Banerjee, M., Basu, R.K., & Das S.K. Cu (II) removal using green adsorbents: 585  
kinetic modeling and plant scale-up design. *Environ. Sci. Poll. Res.* **26**(12), 11542- 586  
11557 (2019). 587
3. Dulla, J.B., Tamana, M.R., Boddu, S., Pulipati, K. & Srirama, K. Biosorption of 588  
copper (II) onto spent biomass of *Gelidiella acerosa* (brown marine algae): 589  
optimization and kinetic studies. *Appl. Water Sci.* **10**(2), 1-10 (2020). 590
4. Calero, M., Iáñez-Rodríguez, I., Pérez, A., Martín-Lara, M.A. & Blázquez, G. 591  
Neural fuzzy modelization of copper removal from water by biosorption in fixed- 592  
bed columns using olive stone and pinion shell. *Bioresour. Technol.* **252**,100–109 593  
(2018). 594

5. Al-Homaidan, A. A., Al-Houri, H. J., Al-Hazzani, A. A., Elgaaly, G. & Moubayed, N. M. Biosorption of copper ions from aqueous solutions by *Spirulina platensis* biomass. *Arabian J. Chem.* **7**(1), 57-62 (2014).
6. Chen, H. & Wang, A. Kinetic and isothermal studies of lead ion adsorption onto palygorskite clay. *J. Colloid Interface Sci.* **307**, 309–316 (2007).
7. Ramos-Vargas, S., Huirache-Acuña, R., Guadalupe Rutiaga-Quiñones, J. & Cortés-Martínez, R. Effective lead removal from aqueous solutions using cellulose nanofibers obtained from water hyacinth. *Water Supply.* **20**(7), 2715-2736 (2020).
8. Lindholm-Lehto, P.. Biosorption of heavy metals by lignocellulosic biomass and chemical analysis. *BioResources.* **14**(2), 4952–4995 (2019).
9. Fawzy, M.A., Hifney, A.F., Adam, M.S. & Al-Badaani, A.A. Biosorption of cobalt and its effect on growth and metabolites of *Synechocystis pevalekii* and *Scenedesmus bernardii*: Isothermal analysis. *Environ. Technol. Innov.* 100953 (2020).
10. Asemave, K., Thaddeus, L. & Tarhembra, P.T. Lignocellulosic based sorbents: A Review. *Sustainable Chem.* **2**, 271–285 (2021).
11. Alia, R.M., Hamada, H.A., Hussein, M.M. & Malash, G.F. Potential of using green adsorbent of heavy metal removal from aqueous solutions: Adsorption kinetics, isotherm, thermodynamic, mechanism and economic analysis. *Ecol. Eng.* **91**, 317–332 (2016).
12. Medhi, H., Chowdhury, P.R., Baruah, P.D. & Bhattacharyya, K.G. Kinetics of Aqueous Cu(II) Biosorption onto *Thevetia peruviana* Leaf Powder. *ACS omega.* **5**(23), 13489-13502 (2020).

13. Nasir, M.H., Nadeem, R., Akhtar, K., Hanif, M.A. & Khalid, A.M. Efficacy of modified distillation sludge of rose (*Rosa centifolia*) petals for lead (II) and zinc (II) removal from aqueous solutions. *J. Hazard. Mater.* **147**(3), 1006-1014 (2007).
14. Iftikhar, A.R., Bhatti, H.N., Hanif, M.A. & Nadeem, R. Kinetic and thermodynamic aspects of Cu (II) and Cr (III) removal from aqueous solutions using rose waste biomass. *J. Hazard. Mater.* **161**(2-3), 941-947 (2009).
15. Ansari, T.M. *et al.* Immobilization of rose waste biomass for uptake of Pb (II) from aqueous solutions. *Biotechnol. Res. Inter.* (2011). doi:10.4061/2011/685023.
16. Aman, A., Ahmed, D., Asad, N., Masih, R. & Abd ur Rahman, H.M. Rose biomass as a potential biosorbent to remove chromium, mercury and zinc from contaminated waters. *Inter. J. Environ. Stud.* **75**(5), 774-787 (2018).
17. Kumar, S.S. & Bishnoi, N.R. Coagulation of landfill leachate by FeCl<sub>3</sub>: process optimization using Box–Behnken design (RSM). *Appl. Water Sci.* **7**, 1943–1953 (2017).
18. Fawzy, M.A. Fatty acid characterization and biodiesel production by the marine microalga *Asteromonas gracilis*: statistical optimization of medium for biomass and lipid enhancement. *Mar. Biotechnol.* **19**(3), 219-231 (2017).
19. Fawzy, M.A. & Alharthi, S. Use of Response Surface Methodology in optimization of biomass, lipid productivity and fatty acid profiles of marine microalga *Dunaliella parva* for biodiesel production. *Environ. Technol. Innov.* **22**,101485 (2021).
20. Mohd Salleh, M.A., Mahmoud, D.K., Wan AbdulKarim, W.A. & Idris, A. Cationic and anionic dye adsorption by agricultural solid wastes: a comprehensive review. *Desalination.* **280**, 1–13 (2011).

21. Chen, X., Tian, Z., Cheng, H., Xu, G. & Zhou, H. Adsorption process and mechanism of heavy metal ions by different components of cells, using yeast (*Pichia pastoris*) and Cu<sup>2+</sup> as biosorption models. *RSC Advances*. **11**(28), 17080-17091 (2021).
22. Fawzy, M.A. Biosorption of copper ions from aqueous solution by *Codium vermilara*: optimization, kinetic, isotherm and thermodynamic studies. *Adv. Powder Technol.* **31**(9), 3724-3735 (2020).
23. Dehghani, H.M. *et al.* Response surface modeling, isotherm, thermodynamic and optimization study of arsenic (V) removal from aqueous solutions using modified bentonite-chitosan (MBC). *Korean J. Chem. Eng.* **32**,1–11 (2016).
24. Bibi, A., Naz, S. & Uroos, M. Evaluating the Effect of Ionic Liquid on Biosorption Potential of Peanut Waste: Experimental and Theoretical Studies. *ACS omega*. **6**, 22259–22271 (2021).
25. Fawzy, M.A. & Alharthi, S. Cellular responses and phenol bioremoval by green alga *Scenedesmus abundans*: Equilibrium, kinetic and thermodynamic studies. *Environ Technol. Innov.* **22**,101463 (2021).
26. Ghasemi, M., Naushad, M., Ghasemi, N. & Khosravi-Fard, Y. Adsorption of Pb (II) from aqueous solution using new adsorbents prepared from agricultural waste: adsorption isotherm and kinetic studies. *J. Indust. Eng. Chem.* **20**(4), 2193-2199 (2014).
27. Meitei, M.D. & Prasad, M.N.V. Adsorption of Cu(II), Mn(II) and Zn(II) by *Spirodela polyrhiza* (L.) Schleiden: equilibrium, kinetic and thermodynamic studies. *Ecol. Eng.* **71**, 308-317 (2014).
28. Fawzy, M.A. & Gomaa, M. Use of algal biorefinery waste and waste office paper in the development of xerogels: A low cost and eco-friendly biosorbent for the

- effective removal of congo red and Fe (II) from aqueous solutions. *J. Environ. Manag.* **262**, 110380 (2020). 667  
668
29. Thanthri, S.H.P., Ranaweera, K.H. & Perera, B.A. Adsorption Study of Cu<sup>2+</sup> Ions 669  
from Aqueous Solutions by Bael Flowers (*Aegle marmelos*). *Biointerface Res. Appl. Chem.* **11**(4),11891-11904 (2021). 670  
671
30. Kalavathy, M.H., Karthikeyan, T., Rajgopal, S. & Miranda, L.R. Kinetic and 672  
isotherm studies of Cu(II) adsorption onto H-activated rubber wood sawdust. *J. Colloid Interface Sci.* **292**, 354–362 (2005). 673  
674
31. King, P., Srinivas, P., Kumar, Y.P. & Prasad, V.S.R.K. Sorption of copper (II) ion 675  
from aqueous solution by *Tectona grandis* L.f. (teak leaves powder). *J. Hazard. Mater.* **136**,560–566 (2006). 676  
677
32. Khormaei, M., Nasernejad, B., Edrisi, M. & Eslamzadeh, T. Copper biosorption 678  
from aqueous solutions by sour orange residue. *J. Hazard. Mater.* **149**, 269-274 679  
(2007). 680
33. Sathasivam, K. & Haris, M.R.H.M. Banana trunk fibers as an efficient biosorbent 681  
for the removal of Cd(II), Cu(II), Fe(II) and Zn(II) from aqueous solutions. *J. Chil. Chem. Soc.* **55**, 278–282 (2010). 682  
683
34. Ai, T. *et al.* Equilibrium, kinetic and mechanism studies on the biosorption of 684  
Cu<sup>2+</sup> and Ni<sup>2+</sup> by sulfur-modified bamboo powder. *Korean J. Chem. Eng.* **32**, 685  
342–349 (2015). 686
35. Abadian, S., Rahbar-Kelishami, A., Norouzbeigi, R. & Peydayesh, M. Cu(II) 687  
adsorption onto *Platanus orientalis* leaf powder: kinetic, isotherm, and 688  
thermodynamic studies. *Res. Chem. Intermed.* **41**, 7669–7681 (2015). 689
36. Vasudevan, S. & Lakshmi, J. The adsorption of phosphate by graphene from 690  
aqueous solution. *RSC Adv.* **2**, 5234–5242 (2012). 691

37. Kumar, N., Mittal, H., Alhassan, S.M. & Ray, S.S. Bionanocomposite Hydrogel 692  
for the Adsorption of Dye and Reusability of Generated Waste for the 693  
Photodegradation of Ciprofloxacin: A Demonstration of the Circularity Concept 694  
for Water Purification. *ACS Sustainable Chem. Eng.* **6**, 17011–17025 (2018). 695
38. Malamis, S. & Katsou, E. A review on zinc and nickel adsorption on natural and 696  
modified zeolite, bentonite and vermiculite: examination of process parameters, 697  
kinetics and isotherms. *J. Hazard. Mater.* **252**, 428-461 (2013). 698
39. Langmuir, I. The adsorption of gases on plane surfaces of glass, mica and 699  
platinum. *J. Am. Chem. Soc.* **40**, 1361–1403 (1918). 700
40. Pavasant, P. *et al.* Biosorption of Cu<sup>2+</sup>, Cd<sup>2+</sup>, Pb<sup>2+</sup>, and Zn<sup>2+</sup> using dried marine 701  
green macroalga *Caulerpa lentillifera*. *Bioresour. Technol.* **97**(18), 2321-2329 702  
(2006). 703
41. Aydın, H., Bulut, Y., & Yerlikaya, Ç. Removal of copper (II) from aqueous 704  
solution by adsorption onto low-cost adsorbents. *J. Environ. Manag.* **87**(1), 37-45 705  
(2008). 706
42. Bazargan-Lari, R., Zafarani, H.R., Bahrololoom, M.E. & Nemati, A. Removal of 707  
Cu(II) ions from aqueous solutions by low-cost natural hydroxyapatite/chitosan 708  
composite: equilibrium, kinetic and thermodynamic studies. *J. Taiwan Institute* 709  
*Chem. Eng.* **45**, 1642–1648 (2014). 710
43. Vijayaraghavan, K., Padmesh, T.V.N., Palanivelu, K. & Velan, M. Biosorption 711  
of nickel(II) ions onto *Sargassum wightii*: Application of two-parameter and 712  
three-parameter isotherm models. *J. Hazard. Mater.* **133**,304–308 (2006). 713
44. Khan, T.A., Mukhlif, A.A., Khan, E.A. & Sharma, D.K. Isotherm and kinetics 714  
modeling of Pb(II) and Cd(II) adsorptive uptake from aqueous solution by 715

- chemically modified green algal biomass. *Model. Earth syst. Environ.* **2**(3), 1-13 716  
(2016). 717
45. Samuel, M.S., Abigail, M.E.A. & Chidambaram, R. Isotherm modelling, kinetic 718  
study and optimization of batch parameters using response surface methodology 719  
for effective removal of Cr(VI) using fungal biomass. *PLoS One.* **10**(3), e0116884 720  
(2015). 721
46. Gupta, V. & Rastogi, A. Biosorption of hexavalent chromium by raw and 722  
acid-treated green alga *Oedogonium hatei* from aqueous solutions. *J. Hazard.* 723  
*Mater.* **163**, 396-402 (2009). 724
47. Bermúdez, Y.G., Rico, I.L.R., Guibal, E., deHoces, M.C. & Lara, M.A.M. 725  
Biosorption of hexavalent chromium from aqueous solution by *Sargassum* 726  
*muticum* brown alga. Application of statistical design for process optimization. 727  
*Chem. Eng. J.* **183**, 68-76 (2012). 728
48. Sathvika, T., Manasi, Rajesh, V. & Rajesh, N. Adsorption of chromium supported 729  
with various column modelling studies through the synergistic influence of 730  
*Aspergillus* and cellulose. *J. Environ. Chem. Eng.* **4** (3), 3193-3204 (2016). 731
49. Hodaifa, G., Alami, S.B.D., Ochando-Pulido, J.M. & Victor-Ortega, M.D. Iron 732  
removal from liquid effluents by olive stones on adsorption column: Breakthrough 733  
curves. *Ecol. Eng.* **73**, 270-275 (2014). 734
50. Asim, A.M., Uroos, M., Naz, S. & Muhammad, N. Pyridinium protic ionic 735  
liquids: Effective solvents for delignification of wheat straw. *J. Mol. Liq.* **325**, 736  
115013 (2021). 737
51. El-Naggar, N.E.A., Hamouda, R.A., Saddiq, A.A. & Alkinani, M.H. Simultaneous 738  
bioremediation of cationic copper ions and anionic methyl orange azo dye by 739  
brown marine alga *Fucus vesiculosus*. *Sci. Rep.* **11**(1), 1-19 (2021). 740

52. Pradhan, D., Sukla, L.B., Mishra, B.B. & Devi, N. Biosorption for removal of hexavalent chromium using microalgae *Scenedesmus* sp. *J. Clean. Prod.* **209**, 617-629 (2019).
53. Grace, C.E.E. *et al.* Biomolecular transitions and lipid accumulation in green microalgae monitored by FTIR and Raman analysis. *Spectrochim. Acta A Mol. Biomol. Spectrosc.* **224**, 117382 (2020).
54. Ponnuswamy, I., Madhavan, S. & Shabudeen, S. Isolation and Characterization of Green Microalgae for Carbon Sequestration, Waste Water Treatment and Bio-fuel Production. *Int. J. Bio-Sci. Bio-Technol.* **5**, 17–26 (2013).
55. Dittert, I.M. *et al.* Adding value to marine macro-algae *Laminaria digitata* through its use in the separation and recovery of trivalent chromium ions from aqueous solution. *Chem. Eng. J.* **193**, 348-357 (2012).
56. Bertagnolli, C., daSilva, M.G.C. & Guibal, E. Chromium biosorption using the residue of alginate extraction from *Sargassum filipendula*. *Chem. Eng. J.* **237**, 362-371 (2014).
57. Wen, Y., Chen, H., Yuan, Y., Xu, N. & Kang, X. Enantioselective ecotoxicity of the herbicide dichlorprop and complexes formed with chitosan in two fresh water green algae. *J. Environ. Monit.* **13**, 879–885 (2011).
58. Stehfest, K., Toepel, J. & Wilhelm, C. The application of micro-FTIR spectroscopy to analyze nutrient stress-related changes in biomass composition of phytoplankton algae. *Plant Physiol. Biochem.* **43**, 717–726 (2005).
59. Elangovan, R., Philip, L. & Chandraraj, K. Biosorption of hexavalent and trivalent chromium by palm flower (*Borassus aethiopum*). *Chem. Eng. J.* **141**, 99-111 (2008).

60. Sultana, N. *et al.* Experimental study and parameters optimization of microalgae based heavy metals removal process using a hybrid response surface methodology-crow search algorithm. *Sci. Rep.* **10**,15068 (2020).
61. Barquilha, C.E.R., Cossich, E.S., Tavares, C.R.G. & Silva, E.A. Biosorption of nickel (II) and copper (II) ions in batch and fixed-bed columns by free and immobilized marine algae *Sargassum* sp. *J. Clean. Prod.* **150**, 58–64 (2017).
62. Tan, K.F., Chu, K.H. & Hashim, M.A. Continuous packed bed biosorption of copper by immobilized seaweed biomass. *ejmp & ep (Eur. J. Min. Proc. Environ. Protec.* **2**, 246–252 (2002).
63. Mata, Y.N., Blázquez, M.L., Ballester, A., González, F. & Munoz, J.A. Biosorption of cadmium, lead and copper with calcium alginate xerogels and immobilized *Fucus vesiculosus*. *J. Hazard. Mater.* **163**(2-3), 555-562 (2009).
64. Davis, T. A., Ramirez, M., Mucci, A. & Larsen, B. Extraction, isolation and cadmium binding of alginate from *Sargassum* spp. *J. Appl. Phycol.* **16**(4), 275-284 (2004).
65. Sadhu, K., Mukherjee, A., Shukla, S.K., Adhikari, K. & Datta, S. Adsorptive removal of phenol from coke-oven waste water using *Gondwana shale*, India: experiment, modeling and optimization. *Desalin. Water Treat.* **52**(34–36),6492–6504 (2014).
66. Kumar, S.S. & Saramma, A.V. Nitrate and phosphate uptake by immobilized cells of *Gloeocapsa gelatinosa*. *J. Mar. Biol. Ass. India.* **54**,119–122 (2012).

## Acknowledgments

The authors extend their appreciation to the Deputyship for Research & Innovation, Ministry of Education in Saudi Arabia for funding this research work through the project number 1-441-129.

<b>Author Contributions</b>	790
M.A.F.: Investigation, formal analysis, writing-original draft. H.M.A., T.M.G.:	791
Writing—original draft, supervision, project administration, funding acquisition,	792
writing—review & editing. M.A.F., R.Z.H., T.G.A.: Methodology, supervision,	793
writing—review & editing. E.F.A.: Methodology, writing—review & editing.	794
<b>Competing interests</b>	795
The authors declare no competing interests.	796
<b>Corresponding author</b>	797
Correspondence to Mustafa A. Fawzy.	798
<b>Figure captions:</b>	799
<b>Fig. 1. 3-D response surface plots for Cu<sup>2+</sup> removal percentage showing the</b>	800
<b>interaction influences of (a) biosorbent dosage and pH, (b) biosorbent dosage and</b>	801
<b>initial copper concentration, and (c) pH and initial copper concentration.</b>	802
<b>Fig. 2. (a) Influence of contact time, (b) Pseudo-first order plot, (c) Pseudo-</b>	803
<b>second order plot, (d) Elovich plot, and (e) Intra-particle diffusion plot for the</b>	804
<b>biosorption of Cu<sup>2+</sup> ions onto <i>R. damascena</i> leaf.</b>	805
<b>Fig. 3. Biosorption isotherms of copper ions onto <i>R. damascena</i> leaf including (a)</b>	806
<b>Langmuir, (b) Freundlich, (c) Temkin, and (d) Dubinin–Radushkevich models.</b>	807
<b>Fig. 4. Plot of <math>1/T</math> against <math>\ln K</math> for copper ions biosorption onto <i>R. damascena</i>.</b>	808
<b>Fig. 5. SEM images of <i>R. damascena</i> leaf (a) before, and (b) after Cd<sup>2+</sup></b>	809
<b>biosorption.</b>	810
<b>Fig. 6. EDX images of <i>R. damascena</i> leaf (a) before, and (b) after Cd<sup>2+</sup></b>	811
<b>biosorption.</b>	812
<b>Fig. 7. FTIR spectra of <i>R. damascena</i> leaf (a) before, and (b) after Cd<sup>2+</sup></b>	813
<b>biosorption.</b>	814



# Figures

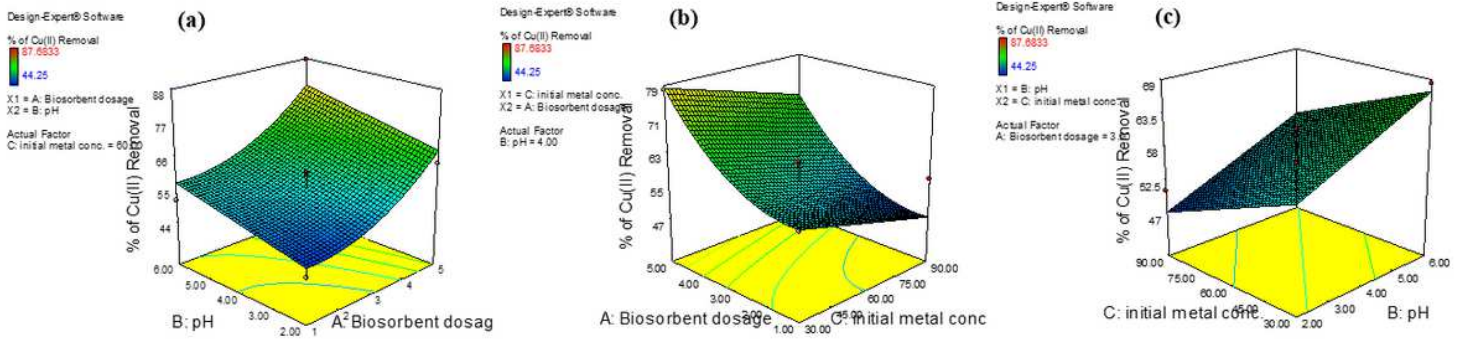
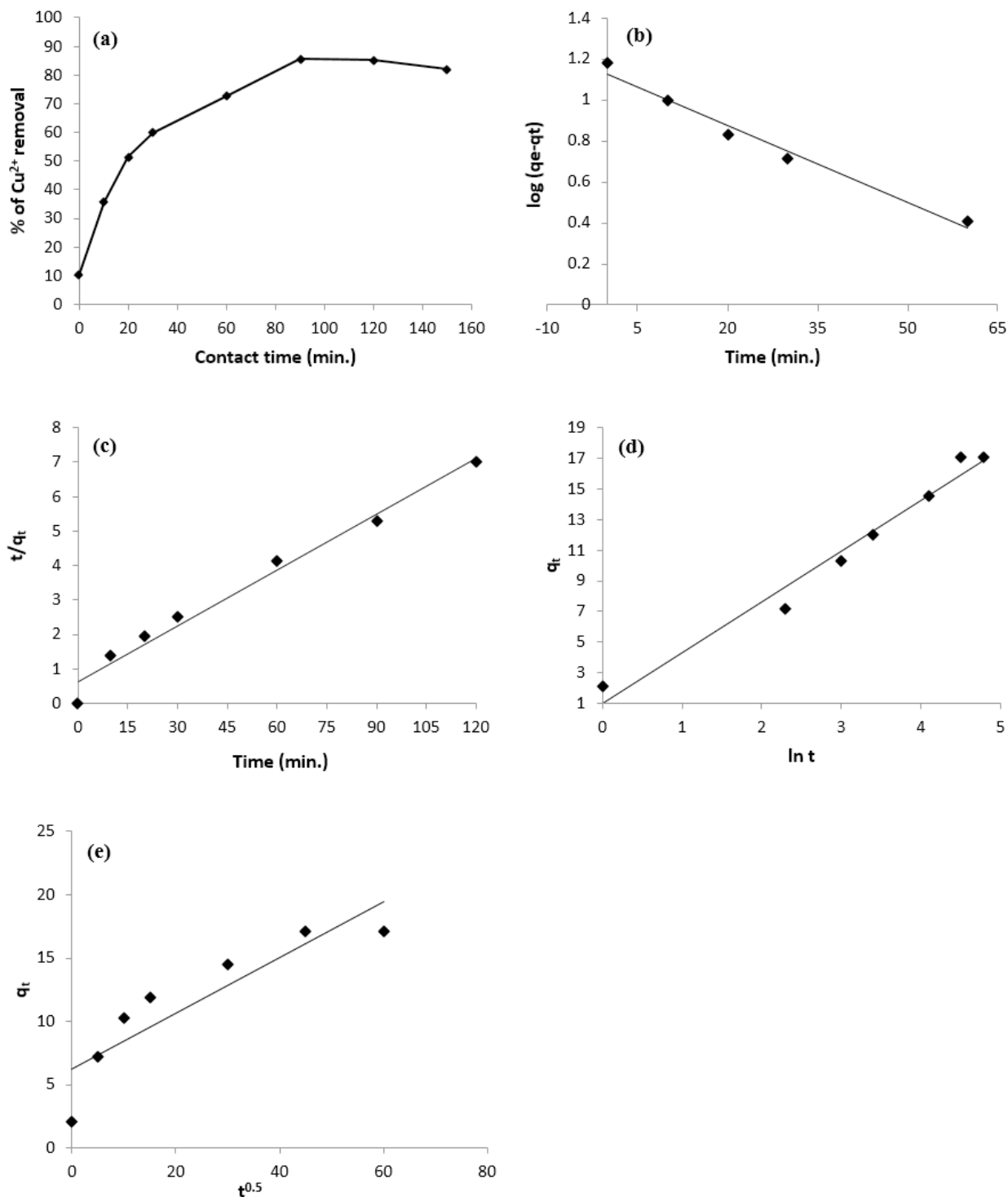


Figure 1

3-D response surface plots for  $\text{Cu}^{2+}$  removal percentage showing the interaction influences of (a) biosorbent dosage and pH, (b) biosorbent dosage and initial copper concentration, and (c) pH and initial copper concentration.



**Figure 2**

(a) Influence of contact time, (b) Pseudo-first order plot, (c) Pseudo-second order plot, (d) Elovich plot, and (e) Intra-particle diffusion plot for the biosorption of  $\text{Cu}^{2+}$  ions onto *R. damascena* leaf.

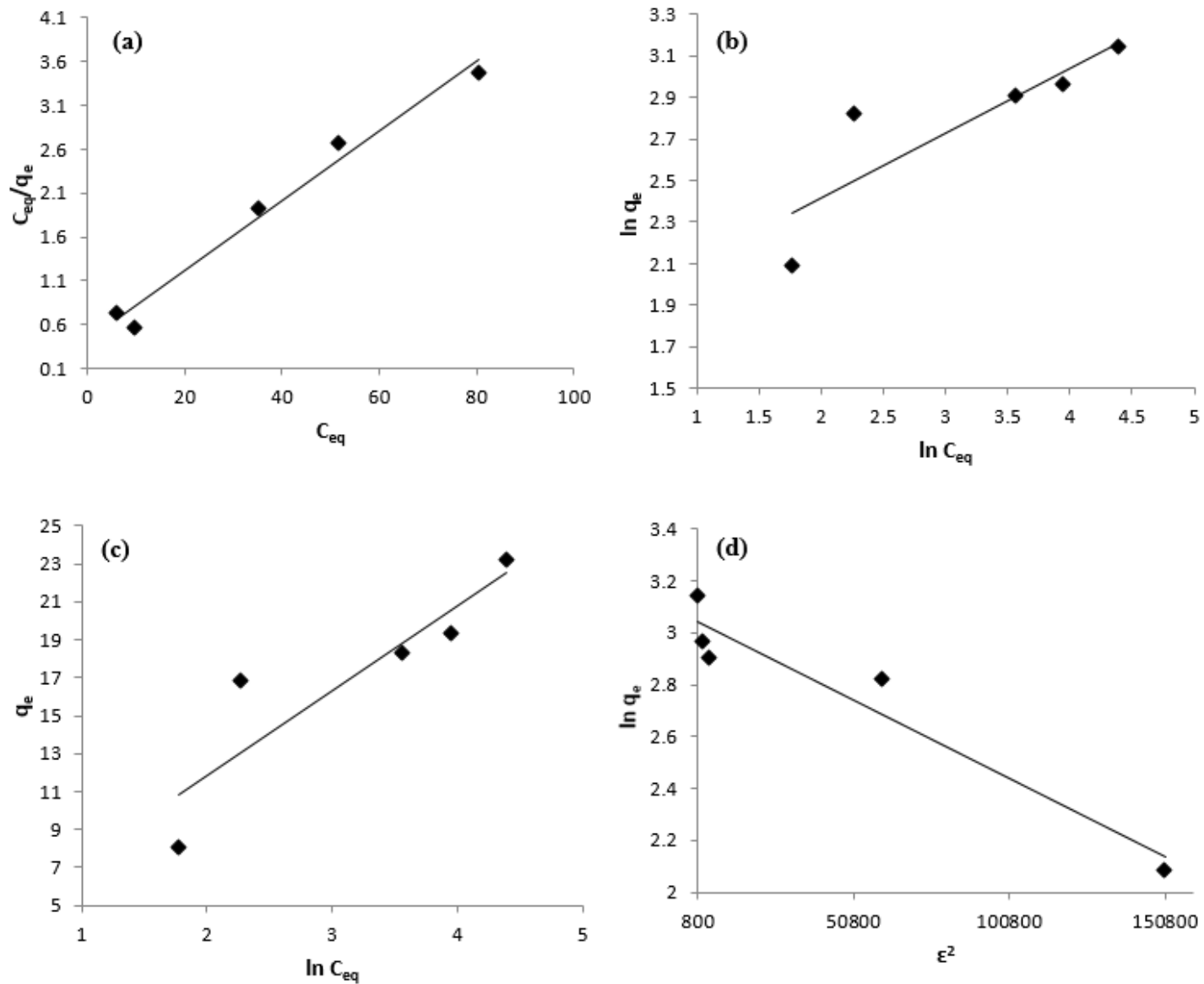


**Figure 3**

Biosorption isotherms of copper ions onto *R. damascena* leaf including (a) Langmuir, (b) Freundlich, (c) Temkin, and (d) Dubinin–Radushkevich models.

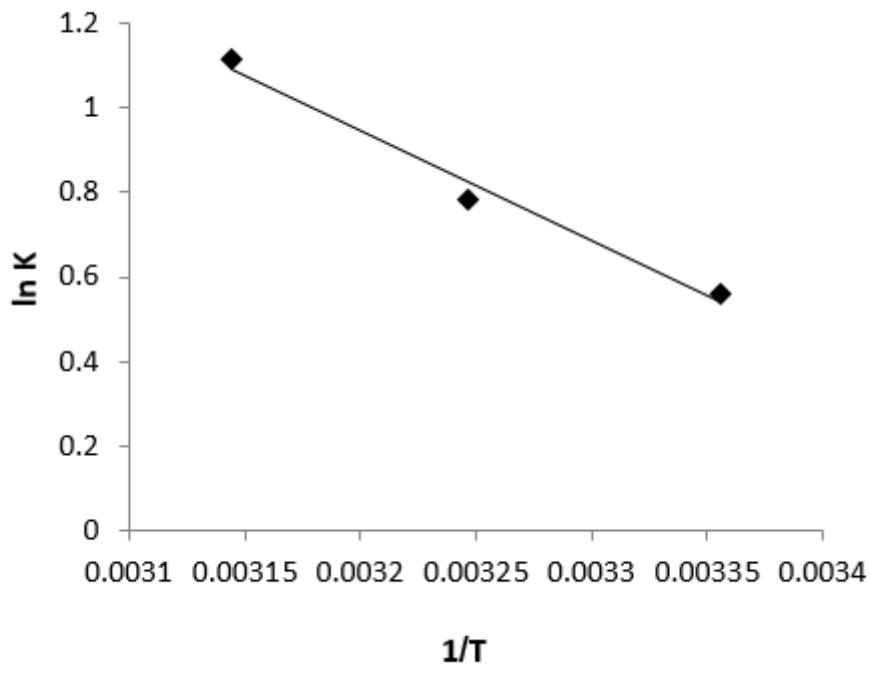


**Figure 4**

Plot of  $1/T$  against  $\ln K$  for copper ions biosorption onto *R. damascena*.

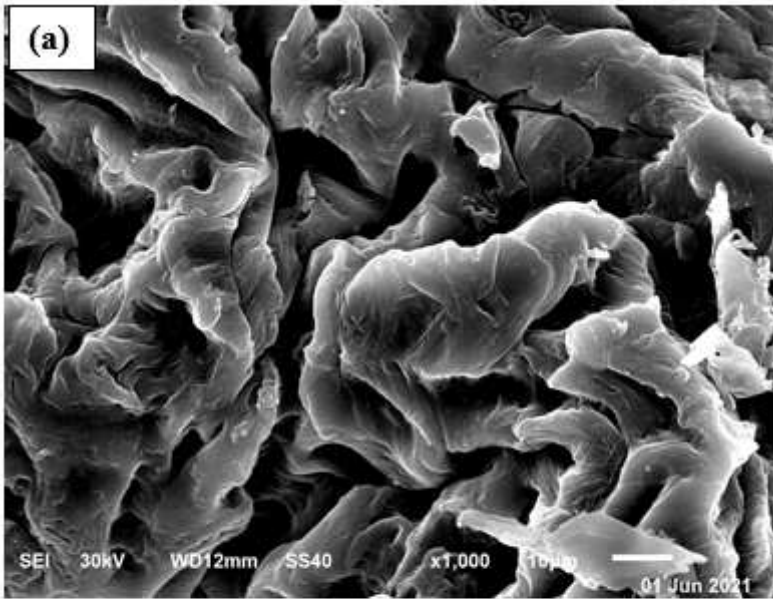


**Figure 5**

SEM images of *R. damascena* leaf (a) before, and (b) after  $\text{Cd}^{2+}$  biosorption.

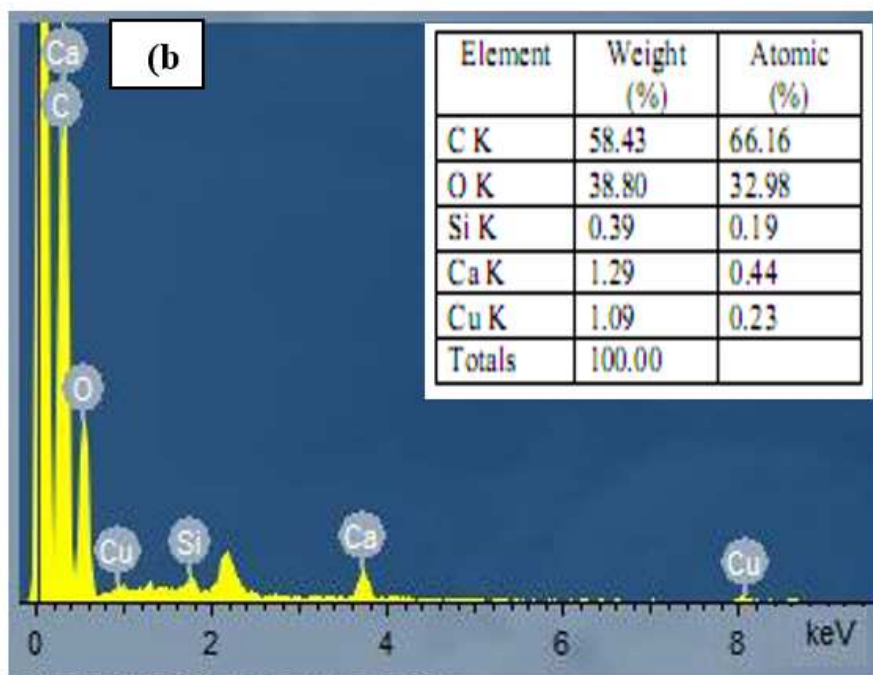
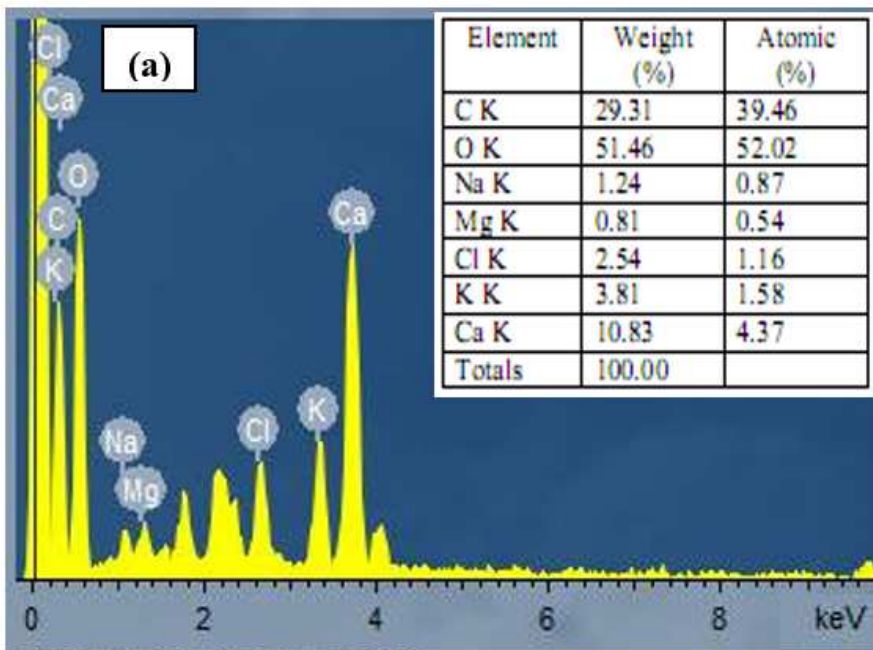


Figure 6

EDX images of *R. damascena* leaf (a) before, and (b) after  $Cd^{2+}$  biosorption.

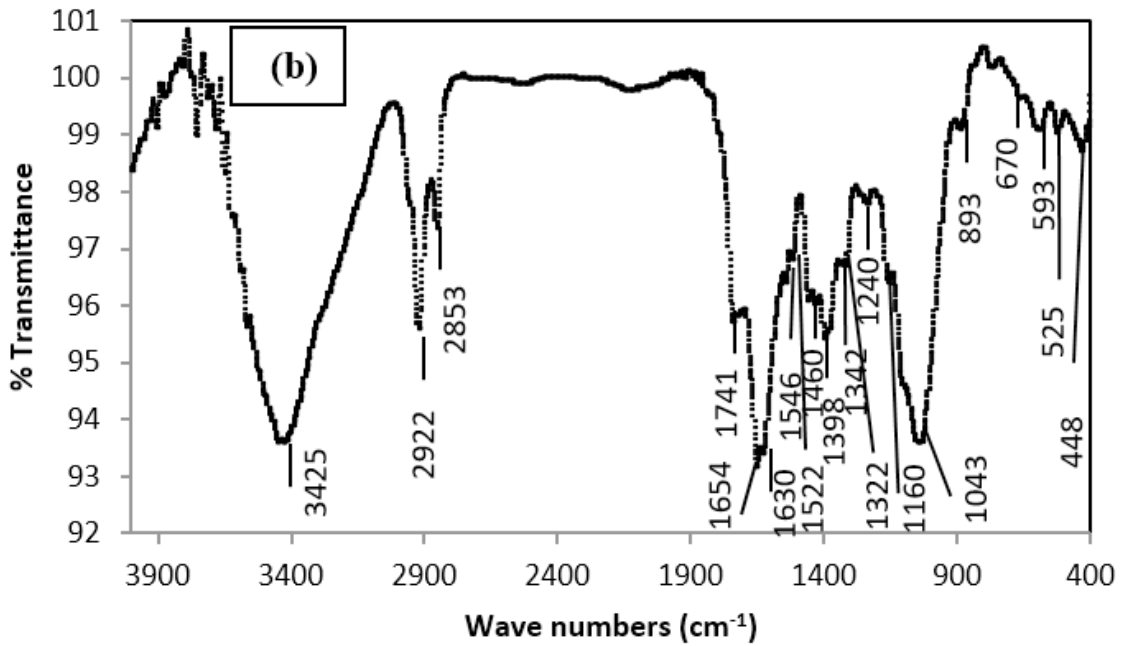
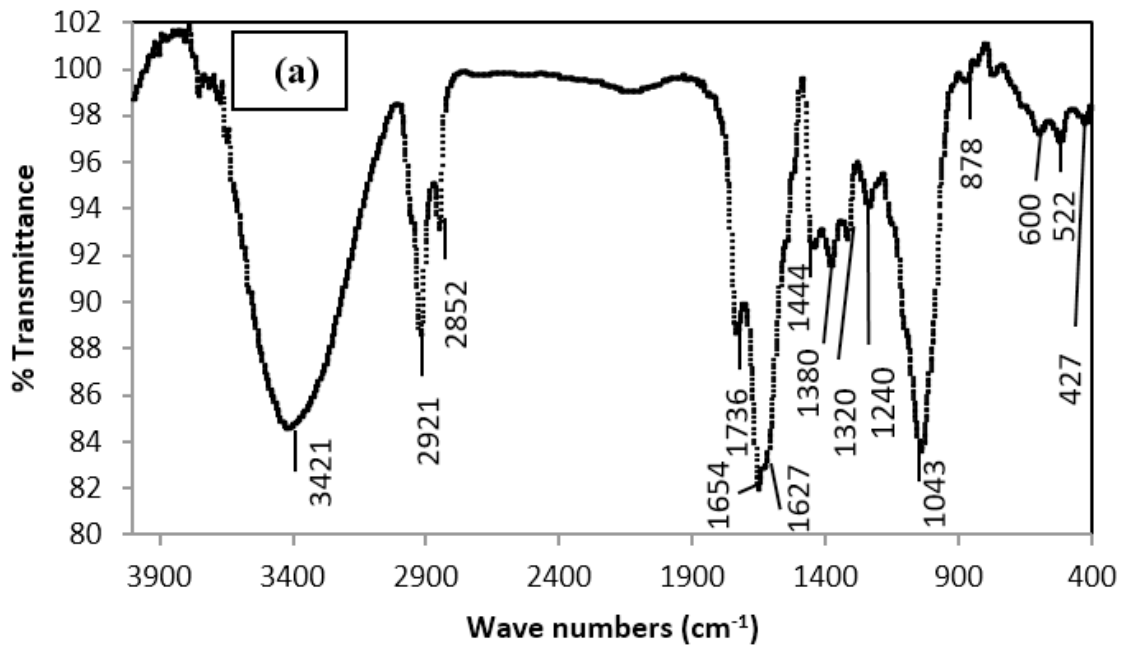


Figure 7

FTIR spectra of *R. damascena* leaf (a) before, and (b) after Cd<sup>2+</sup> biosorption.

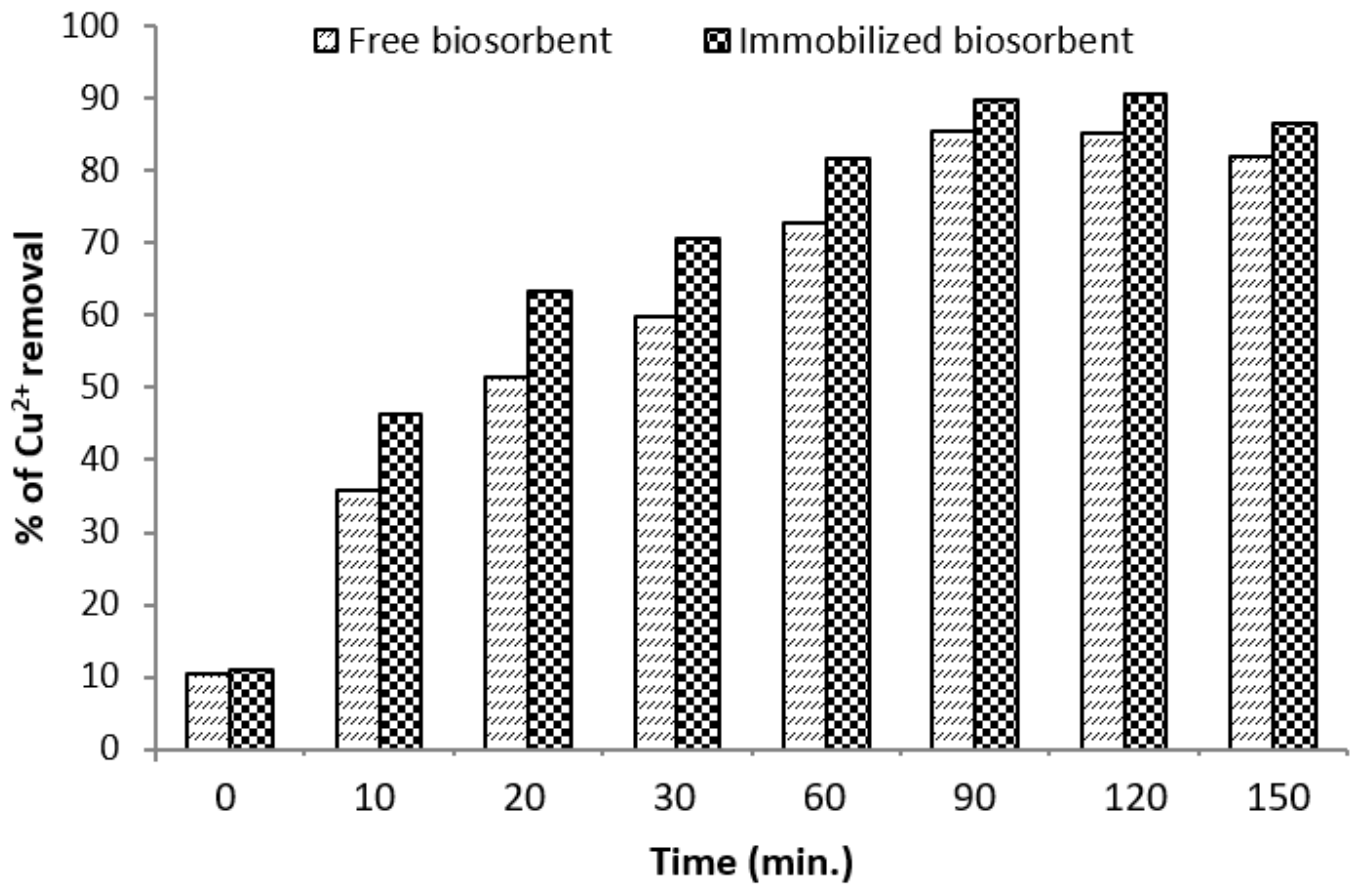


Figure 8

Copper ions removal by Ca-alginate immobilized *R. damascena*.